Automated surface melt detection over the Antarctic from Sentinel-1 imagery using deep learning

Zhu, Qi; Guo, Huadong; Zhang, Lu; Liang, Dong; Wu, Zherong; de Roda Husman, Sophie; Du, Xiaobing

DOI
10.1016/j.jag.2024.103895

Publication date
2024

Document Version
Final published version

Published in
International Journal of Applied Earth Observation and Geoinformation

Citation (APA)
Zhu, Q., Guo, H., Zhang, L., Liang, D., Wu, Z., de Roda Husman, S., & Du, X. (2024). Automated surface melt detection over the Antarctic from Sentinel-1 imagery using deep learning. *International Journal of Applied Earth Observation and Geoinformation*, *130*, Article 103895. https://doi.org/10.1016/j.jag.2024.103895

International Journal of Applied Earth Observation and Geoinformation 130 (2024) 103895

Contents lists available at ScienceDirect

International Journal of Applied Earth Observation and Geoinformation

journal homepage: www.elsevier.com/locate/jag

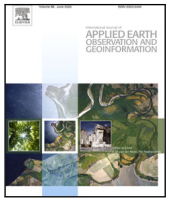

Automated surface melt detection over the Antarctic from Sentinel-1 imagery using deep learning

Qi Zhu [a,b,c], Huadong Guo [b,a,c], Lu Zhang [b,a,c,*], Dong Liang [b,a,c], Zherong Wu [d], Sophie de Roda Husman [e], Xiaobing Du [a,b,c]

[a] Key Laboratory of Digital Earth Science, Aerospace Information Research Institute, Chinese Academy of Sciences, Beijing, 100094, China
[b] International Research Center of Big Data for Sustainable Development Goals, Beijing, 100094, China
[c] University of Chinese Academy of Sciences, Beijing, 100049, China
[d] School of Integrative Plant Science, Soil and Crop Sciences Section, Cornell University, Ithaca, NY, 14850, USA
[e] Department of Geoscience & Remote Sensing, Delft University of Technology, Delft, 2628CN, The Netherlands

ARTICLE INFO

Keywords:
Surface melt detection
Deep learning
Antarctic
Sentinel-1 imagery
Attention DeepLabv3+

ABSTRACT

Surface melt plays a vital role in impacting the polar mass balance and global sea level rise. Over the past decades, synthetic aperture radar (SAR) imagery has garnered considerable attention due to its capacity to provide high-precision and long-term information. However, the traditional SAR-based large-scale surface melt detection methods utilizing co-orbit normalization predominantly depend on reference images and the precise spatial registration to mitigate geometric distortions arising from diverse incidence angles. Consequently, both the absence of reference imagery and the movement of ice sheets and shelves present challenges to the method. In this study, we address this issue by developing a reference-free deep learning network integrating the Convolutional Block Attention Module (CBAM) into DeepLabv3+ to automatically detect surface melt and establishing the surface melt dataset based on multi-temporal Sentinel-1 SAR imagery, encompassing diverse surface conditions of the Antarctic. Our model achieves an accuracy of 95.67%, surpassing the reference-based method and an advanced deep learning-based approach by 4.23% and 4.67%, respectively. Moreover, compared to 500 m resolution UMelt product and the kilometer-level results obtained from Advanced Scatterometer (ASCAT) and Special Sensor Microwave Imager Sounder (SSMIS), our model demonstrates the capability to accurately capture the small-scale melting patterns of ice shelves with a higher spatial resolution of 40 m. Notably, our findings underscore the dispensability of reference imagery in traditional methods through the formidable information extraction capabilities of deep learning. We finally applied the proposed method to extract and analyze the spatiotemporal characteristics of surface melt on the Larsen C Ice Shelf during the 2019/2020 period. The corresponding code of this study is at https://github.com/Tangyu35/Surface-melt-detection.

1. Introduction

The polar ice sheet stands as the largest cold source globally and serves as a highly sensitive indicator of global climate change. Accurately estimating surface melt is crucial for assessing the loss of ice sheet material and surface albedo. In light of the ongoing and accelerating global climate change, there has been a recent increase in the duration and extent of surface melt observed on the Antarctic ice sheet (Jakobs et al., 2021). The consequential accumulation of significant surface meltwater poses a threat to the stability of the ice sheet and its shelves due to resultant changes in stress. Substantial damage resulting from crevasses may trigger natural processes inducing meltwater-induced vertical fracturing, ultimately leading to glacier calving (Arthur et al., 2020). Therefore, precise estimation of surface melt on the ice sheet/shelf is imperative for effectively monitoring ice sheet stability and gaining further insights into its response to global sea level rise (Zhu et al., 2023a).

Over the past two decades, the advancement of earth observation technology has yielded ample data support for polar monitoring,

* Corresponding author at: Key Laboratory of Digital Earth Science, Aerospace Information Research Institute, Chinese Academy of Sciences, Beijing, 100094, China.
E-mail address: zhanglu@aircas.ac.cn (L. Zhang).

https://doi.org/10.1016/j.jag.2024.103895
Received 6 December 2023; Received in revised form 10 April 2024; Accepted 2 May 2024
Available online 16 May 2024

establishing it as a crucial method for detecting surface melt (Liang et al., 2021b). Currently, most surface melt products rely on microwave radiometer and microwave scatterometer images, typically possessing low or medium resolution. Liang et al. (2019) conducted a comprehensive analysis of long-term surface melt in Antarctica and Greenland by leveraging data from Scanning Multichannel Microwave Radiometer (SSMR), Sensor Microwave/Imager (SSM/I) and Special Sensor Microwave Imager Sounder (SSMIS). Their study revealed an upward trend in surface melt on the surface of Greenland and a downward trend in Antarctica, with a certain negative correlation between the two regions. These datasets offer broad coverage and high temporal resolution, rendering them suitable for large-scale and long-duration detection of polar surface meltwater. However, their spatial resolution remains coarse, typically around 25 km or 4.25 km, which poses a challenge for precise detection of surface meltwater and analysis of melting patterns (Benn et al., 2017).

With the increasing availability of medium and high-resolution Synthetic Aperture Radar (SAR) data, known for its effectiveness in overcoming cloud and rain interference, the efficient acquisition of high-resolution surface melt information from ice sheets has emerged as a pressing challenge. SAR, known for its finer resolution and capacity to function independently of weather and illumination conditions, presents a novel approach for surface melt detection. Liang et al. (2021a) developed a co-orbit normalization algorithm utilizing time-series Sentinel-1 images to generate surface melt maps across the pan-Antarctic region. Expanding on this methodology, Hu et al. (2022) applied a similar technique to derive time-series surface melt products in Greenland. However, in the context of implementing SAR data for large-scale surface melt detection, particularly in Antarctica, the complexity of the algorithm often necessitates the utilization of the fixed threshold method (Liang et al., 2021a). Moreover, the need for corresponding reference imagery severely restricts the generalizability of these methods. Given these challenges, there is a pressing demand for a SAR-based reference-free surface melt detection method that offers higher accuracy and a more straightforward processing pipeline

Recently, deep learning has shown superior performance in many computer vision fields (Ma et al., 2024b; Wu et al., 2023). Compared with conventional methods, deep learning methods generate features tailored for the applications automatically, rendering these methods a better choice. SAR imagery is characterized by its substantial volume and intricate features, often accompanied by complex patterns and susceptibility to noise interference and overlapping shadows, which poses challenges that conventional resolution methods struggle to address (Guo et al., 2020). The deep learning technology, leveraging the data-driven nature, presents a promising solution by harnessing a extensive dataset for learning. The networks acquire the ability to discern abstract patterns from vast samples, which enhances the model's capability for generalization, rendering it a highly effective tool for the processing and analysis of SAR images (Zhu et al., 2021). Nevertheless, to the best of our knowledge, there is presently no specialized SAR image database designed explicitly for surface melt detection. This limitation has impeded the progress of deep learning technology within the realm of surface melt detection.

Here, we aim to establish the first deep learning surface melt dataset and introduce an automated framework for surface melt detection using deep learning techniques. We utilize an advanced deep neural network model, DeepLabv3+ (Chen et al., 2018), renowned for its superior performance when compared to other semantic segmentation networks in earth observation applications (Zhang et al., 2021). The DeepLabv3+ architecture integrates an atrous spatial pyramid pooling (ASPP) module, which amalgamates feature information from multiple scales through pooling operations conducted on feature maps. Additionally, DeepLabv3+ accomplishes a significant expansion of the receptive field by utilizing atrous convolutions in contrast to traditional convolutions (Chen et al., 2018). These characteristics make the network well-suited for detecting surface meltwater, as it can precisely capture the distribution and occurrence of surface meltwater at various scales, which varies significantly on different ice shelve (Banwell et al., 2021; Zhu et al., 2023a). However, some surface meltwater is located in complex terrain, such as mountainous high-altitude areas or within radar shadows, making it challenging for deep neural networks to discern these occurrences (Niu et al., 2023). Simultaneously, differing from conventional images in computer vision, remote sensing images typically feature multiple channels and higher resolution. The resulting substantial increase in data volume poses considerable challenges to network performance. Hence, we introduce an attention mechanism that empowers the network to extract relevant and informative features by assigning greater weights to regions of interest, which further bolsters the network's detection meltwater capability (Woo et al., 2018; Ma et al., 2024a). The primary contributions of this work are threefold, as follows:

1. We establish a surface melt detection dataset on the Antarctic based on multi-temporal Sentinel-1 images, includeing 9305 samples and corresponding labels.
2. We propose a fully automated surface melt detection framework using deep learning. The improved DeepLabv3+ network model, combined with the attention mechanism, is applied to detect surface melt.
3. We demonstrate that deep learning effectively overcomes the observation geometry problems caused by satellite orbits and the reliance on reference images of the conventional melt detection framework by intensive experiment.

2. Study area and dataset

2.1. Study sites and Sentinel-1 imagery

The study sites used to train and verify the melt detection algorithm cover the areas in the Antarctic that have undergone intense surface melt. The training and testing sites in our work are selected to ensure (1) the spatial and temporal heterogeneity and diversity within the Antarctic ice shelf region, and (2) encompassing a variety of environments and terrains, including near the grounding line, primary ice shelf regions, and high-altitude mountainous zones, corresponding to different stages of melting (melting start, melting peak, and melting end). Finally, we choose the Larsen C ice shelf (Site 1 in Fig. 1) on Antarctic Peninsula, the Fimbul (Site 2) and Borchgrevink (Site 3) ice shelves in the Queen Maud Land, and the Shackleton ice shelf (Site 4) on East Antarctica. It is worth noting that all study areas are within the Antarctic coastline to eliminate the ocean influence on melt detection.

We collected the Sentinel-1 imagery in Extra Wide (EW) mode with a 40 m spatial resolution for the study sites. The HH polarization products, commonly employed in marine, ice, and polar applications, with an incidence angle ranging from 18.9° to 47.0°, were selected to establish the dataset. The selected training and testing dataset cover the austral summer seasons from 2015 to 2021. Consistent with the spatial distribution of regions, we obtain SAR imagery at different times for every study site. Fig. 2 shows the data distribution of the training dataset where different colors represent four different study sites, and the circle's size represents the data volume's relative size. The Table 1 presented comprehensively illustrates the quantity of Sentinel-1 images utilized for each study site across various temporal intervals. The variations in image numbers across months may arise from differences in image coverage and absence of melting events in certain study sites during specific months.

2.2. Establish surface melt detection dataset

We utilized a rapid and efficient framework for detecting surface melt based on the Google Earth Engine (GEE), harnessing an extensive dataset of Sentinel-1 imagery and employing a co-orbit normalization

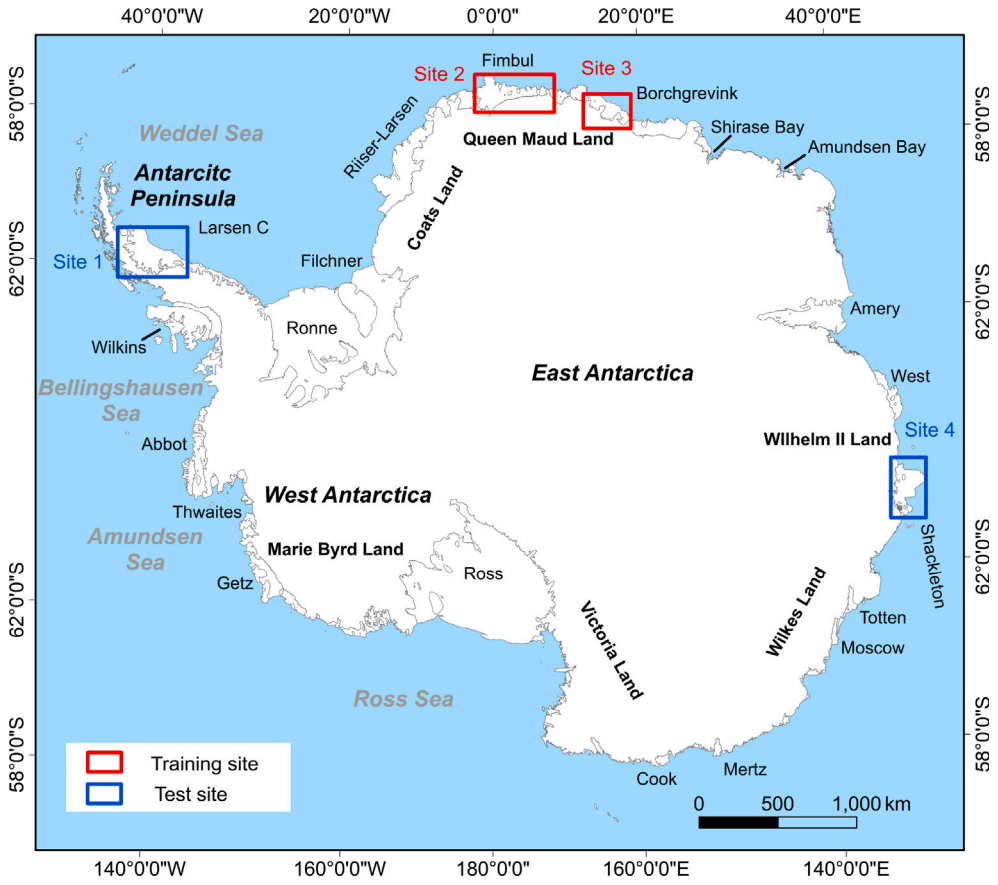

Fig. 1. Spatial distribution of study sites across the Antarctic continent. The Antarctic coastline and ice shelves' boundary are downloaded from Gerrish et al. (2020).

Table 1
Sentinel-1 imagery number of each site in our dataset. Note that the number denotes the total imagery involved in creation the dataset, between which there may be overlap to fully cover the study sites. Therefore, the number of images does not represent the proportion contained in the dataset.

Time (Year–Month)	Site 1 (Larsen C ice shelf)	Site 2 (Fimbul ice shelf)	Site 3 (Borchgrevink ice shelf)	Site 4 (Shackleton ice shelf)
2016-11	0	0	0	4
2016-12	0	48	13	14
2017-01	0	44	22	10
2017-02	0	0	0	10
2017-11	0	0	0	6
2017-12	0	0	9	12
2018-01	0	0	13	33
2018-02	0	0	0	10
2018-10	0	0	22	0
2018-11	40	0	22	8
2018-12	44	0	22	15
2019-01	40	52	38	15
2019-02	0	0	29	9
2019-10	25	0	36	0
2019-11	22	0	31	7
2019-12	28	0	30	26
2020-01	28	49	30	12
2020-02	22	0	0	12

method. Within the GEE platform, the Sentinel-1 data underwent preliminary processing steps, encompassing the elimination of thermal noise, radiometric correction, and rectification for topographic variations (Gorelick et al., 2017). However, for the precise identification of freeze–thaw transitions, further refinement was indispensable, particularly in addressing speckle noise reduction and the elimination of artefacts such as black edges. To address speckle noise, we implemented a boxcar filter, while an entropy value filter was employed to effectively

eliminate areas afflicted by black edges exhibiting low and irregular backscattering coefficients. To achieve a comprehensive coverage of the study area, all images were meticulously merged and subsequently cropped based on the ice shelf boundary.

Following the data preprocessing, the surface melt detection procedure was executed. Variations in incident angles among SAR images posed challenges for surface melt detection due to differing observation geometries. Considering that SAR images captured from the same orbit have the same observation geometry, any change in the backscattering coefficient between winter and summer SAR images will likely be a consequence of melting events on the surface (Liang et al., 2021a). Therefore, we use the co-orbit normalization method to normalize the product imagery with the winter reference imagery from the same orbits. The Eq. (1) represents the formula for the co-orbit normalization.

$$\sigma_{orbit-norm}(x,y) = \sigma_{orbit-study}(x,y)/\sigma_{orbit-ref}(x,y) \quad (1)$$

where, the "orbit" refers to the relative orbit numbers in the GEE Data Catalog, which are restored in the GEE database with the "relativeOrbitNumber" parameter. $\sigma_{orbit-study}(x,y)$, $\sigma_{orbit-ref}(x,y)$ and $\sigma_{orbit-norm}(x,y)$ represent the backscatter coefficient of the SAR data under study at the geographical position, the corresponding location in the winter reference image and the normalized imagery in (x,y) pixels, respectively.

Time filtering was carried out to separate the winter reference images and the study period images for surface melt detection analysis from the entire Sentinel-1 SAR dataset. SAR imagery from June and July for each year were selected as the reference winter images for all years, considering these two months are the coldest time period in Antarctica and do not experience melting (Liang et al., 2019). The other SAR images were selected as the study period images for surface melt detection. Finally, a freeze–thaw image set was obtained using the unified threshold (−2.66 dB, consistent with Liang et al. (2021a) and Zhu et al. (2023a)).

After the surface melt detection, the results of the subsequent surface melt detection were subjected to manual examination and refinement by experienced experts to eliminate potential areas that could lead to misjudgment. We implemented elevation masking (1500 m) to exclude high-altitude regions where melt occurrences are improbable, while ice crevasses and fluctuations in local incidence angle are less frequent (Liang et al., 2021a; de Roda Husman et al., 2024). Additionally, we employed co-orbit normalization with reference imagery to correct geometric distortions. Furthermore, we applied the normalized Radon transform method to identify damaged areas on the Antarctic Ice Shelves (Izeboud and Lhermitte, 2023), thereby eliminating potential sources of interference.

Fig. 3 presents surface melt samples from the Larsen C ice shelf on December 15, 2019, derived from Sentinel-1 images. Overall, the algorithm has successfully obtained precise surface melt distribution information, as depicted in Fig. 3(a) and (d). Fig. 3(b) and (c) showcase regions with ice crevasses on the Larsen C surface (identified in black boxes in Fig. 3(a)) and their corresponding detection results. It is evident that our approach effectively mitigates the impact of ice crevasses on surface melt detection. In areas where surface meltwater occurs within ice crevasses (see Fig. 3(b)), our database accurately annotates them as "Thaw". Conversely, in areas where surface meltwater is absent within ice crevasses (shown in Fig. 3(f)), we correctly label them as "Freeze". Finally, we applied them as our surface melt dataset used to further DL training and testing. Finally, we applied them as our surface melt dataset used to further DL training and testing.

To facilitate training of the network, the post-mosaicking Sentinel-1 images were divided into smaller blocks of size 512 × 512 using a sliding window approach. To preserve the integrity of edge information within the image blocks, a 20% overlap was incorporated between consecutive images. As a result, a first dataset comprising 9305 pairs of SAR images for surface melt detection, along with their corresponding labels, was acquired. The SAR images and labels were saved in the lossless JPEG and PNG format, respectively. The data from the Fimbul (Site 2) and Borchgrevink (Site 3) Ice Shelves are used to train our model, while the imagery from the Larsen C (Site 1) and Shackleton (Site 4) Ice Shelves area employed to test the performance.

Fig. 2. Temporal distribution of Sentinel-1 imagery acquisitions used for automated surface melt extraction, where different colors represent training sites and a test site (red rectangles and the blue rectangle shown in Fig. 1, respectively), and the size of the circle represents the relative size of the data volume. (For interpretation of the references to color in this figure legend, the reader is referred to the web version of this article.)

3. Methodology

Fig. 4 depicts the architecture of the Attention DeepLabv3+ model (Section 3.1.1) containing the attention mechanism (Section 3.1.2) to explore surface melt information extraction based on multi-temporal SAR images. ResNet (Section 3.2.1) and MobileNetV3 backbone (Section 3.2.2) are implemented to extract semantic information from the input imagery, where the former is a classic backbone in the computer vision field, while the latter is a novel architecture focusing on lightweight deep neural network design. In Section 3.3, we introduced five evaluation indexes.

3.1. Attention DeepLabv3+

3.1.1. DeepLabv3+ model

DeepLabv3+, a state-of-art deep neural network model for semantic segmentation adopts the encoder–decoder structure where the encoder captures multi-scale features, and the decoder recovers the image resolution (Fig. 4). Atrous convolution is utilized within the ASPP to specifically manage the output feature map resolution and modify the field-of-view (FOV) without increasing the parameter count. It could precisely capture object boundaries by obtaining multi-scale contextual information and has been widely employed to many remote sensing segmentation missions (Wang et al., 2021; Du et al., 2021).

3.1.2. Attention mechanism

The attention mechanism can increase the representation power of networks by learning contextual information and analyzing the internal correlation. The main idea of it is to increase the weights of meaningful information and ignore the irrelevant (Woo et al., 2018). The attention mechanism has been extensively exploited for designing modern deep neural network architectures (Zhu et al., 2023b). In this study, CBAM, shown in Fig. 5, consisting of a channel attention module (CAM) and a spatial attention module (SAM), is incorporated in the DeepLabv3+ model (namely, Attention DeepLabv3+), where the former focuses on "what" is helpful in a given feature map $\boldsymbol{U}$ and the latter aims to find "where" the meaningful information is.

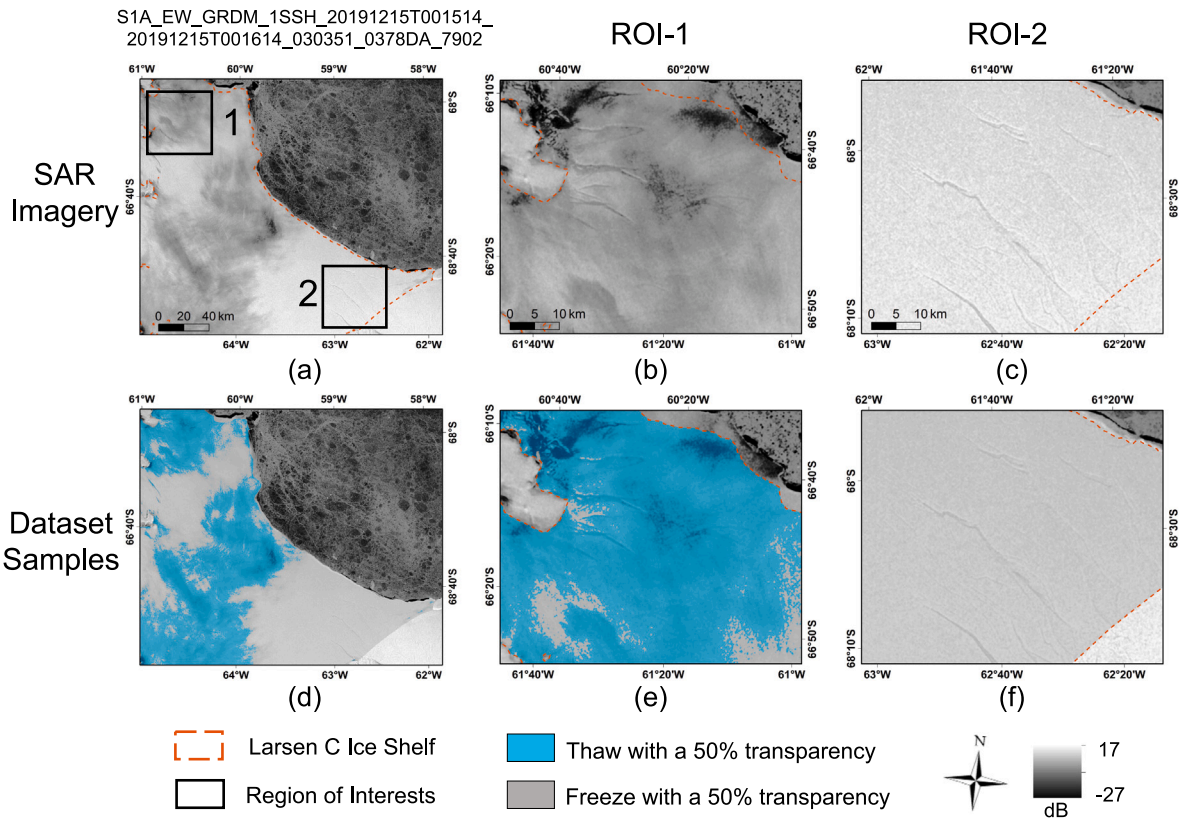

Fig. 3. Surface melt dataset samples (SAR imagery and corresponding results) from the Larsen C Ice Shelf (Site 1 in Fig. 1) used to train the deep learning model where the blue and gray colors represent the thaw and freeze, both of which are with a 50% transparency to display the SAR imagery. Panels (b) and (e) depict regions with ice crevasses highlighted in the black boxes in panel (a). (For interpretation of the references to color in this figure legend, the reader is referred to the web version of this article.)

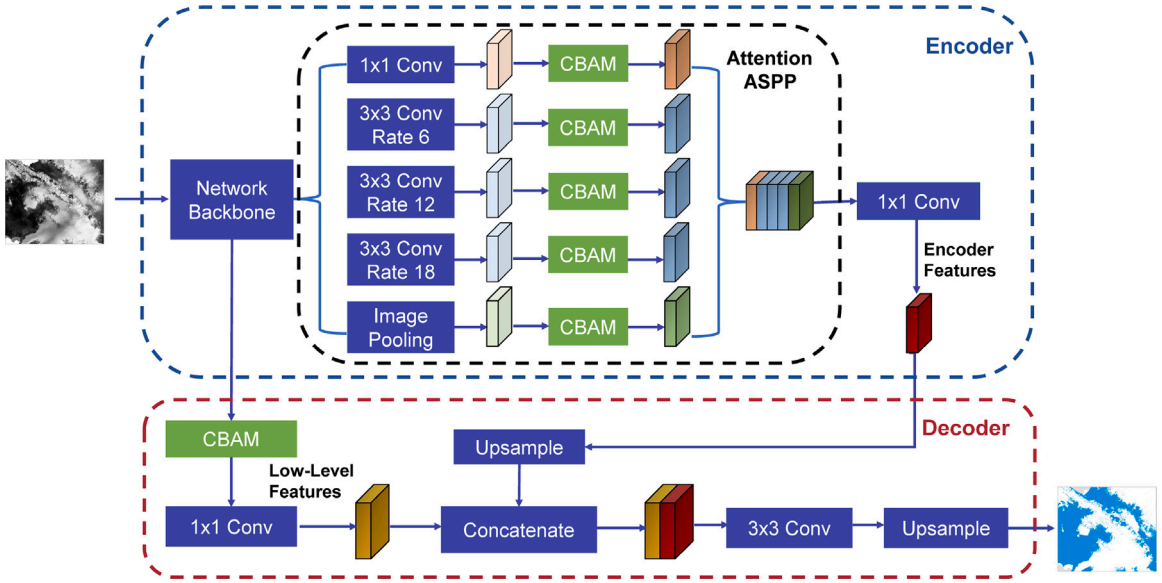

Fig. 4. Architecture of the proposed Attention DeepLabv3+.

In our model, the CBAM is integrated after each parallel atrous convolution in the ASPP layer obtained by atrous convolution from different scales. It is also placed before the low-level feature extraction in the Decoder to capture the rich contextual information derived from the Backbone (Fig. 4).

3.2. Backbone

3.2.1. ResNet

The residual block attempts to solve the gradient explosion and the higher requirement for computation resources by training the

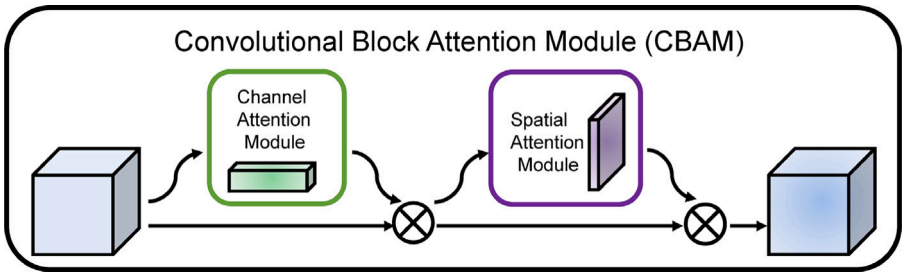

Fig. 5. The overview of the Convolutional Block Attention Module (CBAM).
Source: This figure is adapted from Woo et al. (2018).

additional layers as an identity function ($f(x) = x$) (He et al., 2016). The residual block profoundly influences the design of modern deep neural networks (Vaswani et al., 2017). The main branch of the residual block stacks two 3 × 3 convolutional layers. A Batch Normalization (BN) layer is placed after the convolutional layer and a ReLU activation function (Nair and Hinton, 2010) follows the first BN layer. Meanwhile, the residual block includes a residual connection that directly feeds the input layer x to the addition operator, through which the inputs can forward propagation faster across layers.

3.2.2. MobileNetV3

The Google proposed a lightweight network MobileNet for balancing computation performance in 2017, and accuracy, which has three versions. Here, we provide a general review of the MobileNetV3 (Howard et al., 2019; Hu et al., 2018). Depthwise separable convolution proposed in MobileNetV1 is implemented in MobileNetV3 for each channel of the input feature, significantly reducing the computation resource and model size. Compared with MobileNetV1 and MobileNetV2, MobileNetV3 adopts a novel nonlinear activation function (hard-swish, defined in Eq. (2)), and a powerful network architectural, Squeeze and Excitation block.

$$hard\text{-}swish(x) = x\frac{ReLU6(x+3)}{6} \tag{2}$$

3.3. Evaluation index

Five evaluation metrics are utilized to evaluate the learning ability of Attention DeepLabv3+ models, namely Pixel accuracy, Mean Intersection of Union (MIoU), Precision, Recall, and F_1 score. Pixel accuracy simply reflects the proportion of correctly segmented samples in the imagery. Intersection of Union (IoU) represents the intersection of the detection result and the ground truth to their union, and MIoU is the average IoU of all predicted classes. Precision refers to correctly predicted pixels to all detected ones, while Recall indicates the percentage of correctly predicted masks to the positive. Finally, F_1 score is calculated based on the Precision and Recall. For a more detailed description of the indexes, the authors recommend He et al. (2022).

3.4. Implementation details

We use a central processing unit (CPU) with processor Inter(R) Xeon(R) Gold 6226R (2.69 GHz), a graphics processing unit (GPU) with RTX 8000 with 48G memory in total, and python programming implementation. The PyTorch framework is applied under the Linux system. The largest batch size for each backbone is used to fully utilize the GPU's power (32 for the ResNet backbone and 64 for the MobileNet backbone). We opted for the binary cross-entropy as our loss function and conducted training for each model over 100 epochs. The learning rate was set to 0.005, employing an adaptive decay value of 1e−4, in line with the original implementation of DeepLabv3+ (Chen et al., 2018).

Table 2
Comparison of the performance (%) and computation cost between DeepLabv3+ configured with ResNet and MobileNet backbone on the test set.

Backbone	CBAM	PA	MIoU	Precision	Recall	F_1	Para.
ResNet	✓	**95.47**	**91.09**	**95.42**	**95.25**	**95.34**	40.28M
	✗	93.65	87.75	93.60	93.34	93.47	39.75M
MobileNet	✓	**95.67**	**91.45**	**95.47**	**95.58**	**95.53**	11.25M
	✗	94.08	88.55	94.12	93.74	93.93	11.13M

Table 3
Comparison of the performance (%) and computation cost between DeepLabv3+ configured with ResNet and MobileNet backbone on the training set.

Backbone	CBAM	PA	MIoU	Precision	Recall	F_1	Para.
ResNet	✓	**95.97**	**92.00**	**95.93**	**95.73**	**95.83**	40.28M
	✗	94.37	89.02	94.35	94.03	94.19	39.75M
MobileNet	✓	**96.34**	**92.67**	**96.13**	**96.25**	**96.19**	11.25M
	✗	95.08	90.34	95.13	94.73	94.93	11.13M

4. Experiments results

4.1. Accuracy assessment and ablation study

In our study, we utilized ResNet and MobileNetV3 backbones to extract contextual information from SAR imagery, while integrating CBAM into the DeepLabv3+ model to capture attention weights in both channel and spatial dimensions. To assess the efficacy of these modules, we performed ablation experiments. The evaluation metrics of diverse melt detection models are summarized in Table 2 (on test set) and Table 3 (on training set).

The ablation experiments were conducted on the surface melt dataset. Deep learning-based surface melt detection has demonstrated remarkable accuracy on test set, particularly when incorporating CBAM. The MIoU surpasses 0.91, while the F_1 score exceeds 0.95. Specifically, MobileNetV3-DeepLabv3+ achieves the highest MIoU of 0.9145 and F_1 score of 0.9553. This model effectively utilizes the channel and spatial attention obtained through CBAM, in conjunction with the MobileNet backbone's efficient extraction of low-level features.

4.1.1. The impact of CBAM module

Based on the test set (Table 2), the incorporation of CBAM has a positive impact on surface melt detection accuracy. Specifically, CBAM integration yields a MIoU of 0.9109 and an F_1 score of 0.9534, resulting in a notable improvement of 3.34% and 1.87% in the ResNet-DeepLabv3+ model, respectively. In the case of the MobileNetV3 backbone, the application of CBAM leads to a 2.90% boost in the MIoU metrics, further confirming the enhanced expressiveness of the network due to CBAM and its subsequent improvement in melt detection accuracy.

Additionally, it is noteworthy that, owing to the adaptable nature of the CBAM module and its lightweight design, despite the significant enhancement in model accuracy, computational expenses and training

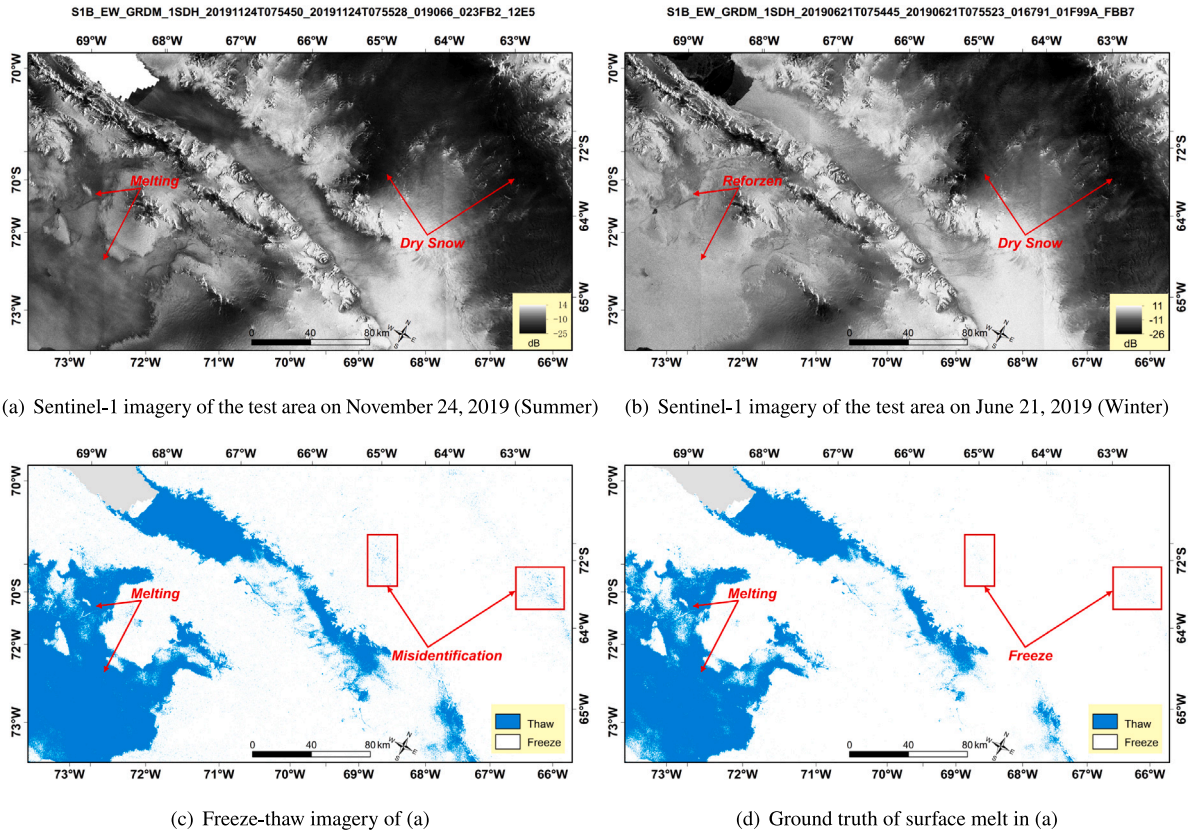

(a) Sentinel-1 imagery of the test area on November 24, 2019 (Summer)

(b) Sentinel-1 imagery of the test area on June 21, 2019 (Winter)

(c) Freeze-thaw imagery of (a)

(d) Ground truth of surface melt in (a)

Fig. 6. Backscatter echo characteristics, the surface melt detection result and the corresponding ground truth of Antarctic ice sheet. The SAR images are stretched using histogram equalize method in ArcMap. Legend—black: no image or masked by elevation, blue: thaw and white: freeze. (For interpretation of the references to color in this figure legend, the reader is referred to the web version of this article.)

duration have only seen a slightly increase. The total parameter increments for the ResNet and MobileNet backbones were a mere 0.53M and 0.12M respectively, representing a mere 1.33% and 1.07% increase.

4.1.2. The impact of network backbone

ResNet and MobileNetV3 backbones were employed to evaluate the model's performance. According to Table 2, MobileNetV3 exhibits a slight performance advantage over the ResNet backbone in melt detection. When applying CBAM, MobileNet achieved a 0.36% improvement in the MIoU metric compared to ResNet. However, when CBAM was not applied, there was a 0.80% improvement. This enhancement is due to the SE block utilized in MobileNetV3 (Howard et al., 2019), which still provides partial attention mechanisms when CBAM is absence.

More meaningfully, MobileNetV3's primary focus on lightweight network design provides evident advantages in inference speed. Based on our experiments (with implementation details matching Section 3.4), the ResNet-DeepLabv3+ model achieves a frame rate of 23.88 frames per second (FPS), whereas the MobileNetV3-based model is capable of inferring 85.16 images per second, which is 3.56 times faster than ResNet-DeepLabv3+.

4.2. Melt detection performance on different ice sheet surface conditions

The dry snow area, melting area, and refreeze area represent three distinct surface environments (Liang et al., 2021a). Fig. 6 visually presents the detection results achieved by our algorithm under these aforementioned surface conditions, providing corresponding SAR imagery and ground truth values. The primary objective is to virtually demonstrate the changes in SAR backscattering characteristics before and after surface melt. The co-orbit normalization method ensures that observational geometry between the reference and experimental SAR imagery are approximately identical by acquiring them from the same orbit of the Sentinel-1 satellite. In the SAR images, the C-band electromagnetic waves effortlessly penetrate the small-sized dry snow, resulting in weak echoes and forming deep black regions (Figs. 6(a) and 6(b)). Conversely, the presence of liquid water generated by melting exerts a substantial absorption effect on electromagnetic waves, leading to a pronounced decrease in backscattering echoes and the appearance of darker areas in the image (Fig. 6(a)). Consequently, differentiating these dry snow regions from the surface melt area, particularly in high-altitude regions, presents a significant challenge due to their similar backscatter coefficients. Fig. 6(c) showcases the detection outcomes obtained from the test site. Our method accurately identifies the frozen area, with an accuracy of 95.67%, particularly in ice shelf regions, as it exhibits distinct backscatter echoes that differ significantly from other areas and performed well in high-altitude mountainous regions, which is typically challenging due to their low backscattering echoes, as well as the presence of overlap and radar shadows at high altitudes.

5. Discussion

5.1. Comparison with other surface melt methods

The Table 4 presents a comparative analysis between our method and various surface melt detection methods, focusing on the data sources, spatiotemporal resolution, and detection accuracy. The Fig. 7 showcases our detection findings in comparison to results obtained through various methods. These methods encompass UMelt, a deep learning method based on U-Net (de Roda Husman et al., 2024), outcomes obtained through the Advanced Scatterometer (ASCAT) (Wang et al., 2022) and results derived from SSMIS data (Trusel et al., 2012).

The surface melt detection from ASCAT (Fig. 7(b)) and SSMIS (Fig. 7(c)) captures the majority of melting patterns on the Shackleton

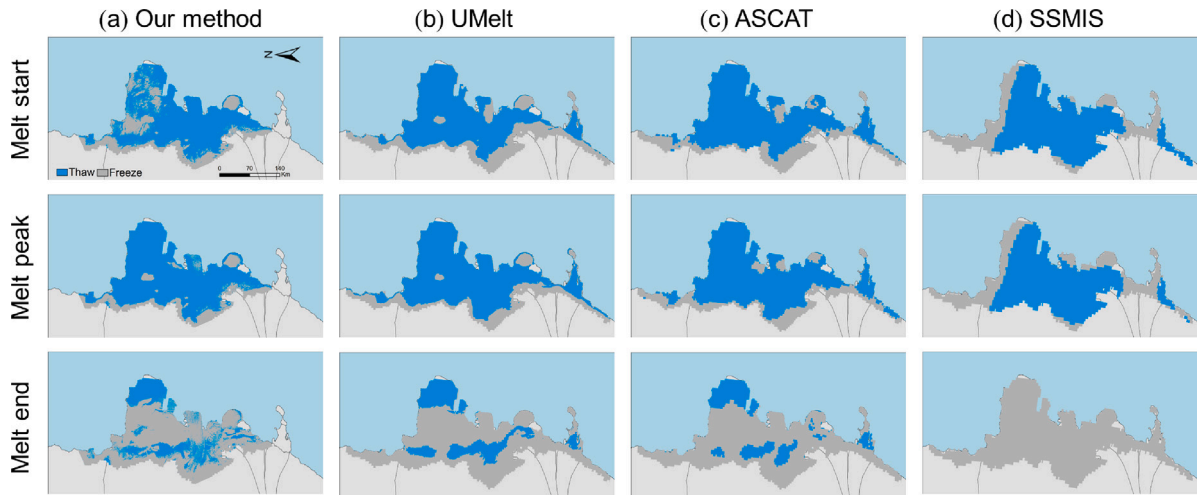

Fig. 7. Qualitative comparison of surface melt on the Shackleton Ice Shelf during the 2016–2017 melt season, including (a) our results, (b) UMelt, (c) ASCAT, and (d) SSMIS at the beginning (30 November 2016), peak (17 January 2017), and end (16 February 2017).
Source: The comparative results for UMelt, ASCAT, and SSMIS are provided by de Roda Husman et al. (2024).

Table 4
Comparison with existing surface melt detection methods. (FH: Fixed threshold, AOT: Adaptive optimal threshold, BTM: Brightness temperature method, IWTM: Improved wavelet-transform method, EDM: Edge detection method, CON: co-orbit normalization and DL: deep learning)

Surface melt detection method	Data source	Spatial resolution	Temporal resolution	Overall accuracy
BTM with FH (Bergeron et al., 2014)	AMSR-E and AMSR-2	12.5 km	Daily	83.30%
IWTM with AOT (Liang et al., 2019)	SMMR, SSM/I and SSMIS	25 km	Daily	82.57%
EDM with AOT (Wang et al., 2018)	SSM/I and QuikSACT	25 km	Daily	81.00%
EDM with FH (Antropova et al., 2022)	RADARSAT-2 SAR	4.8 m	Every 6 days	83.91%
CON with FH (Liang et al., 2021a)	Sentinel-1 SAR	40 m	Every 6 days	91.2%
DL with U-Net (de Roda Husman et al., 2024)	Sentinel-1, ASACT and SSMIS	500 m	Daily	91.0%
Our method	Sentinel-1 SAR	40 m	Every 6 days	**95.67%**

Ice Shelf. However, it appears that SSMIS underestimates surface meltwater in the western region of the Shackleton Ice Shelf. Despite offering high temporal resolution with daily data collection, these methods suffer from relatively coarse spatial resolution, posing a significant challenge in accurately capturing minor melting patterns (de Roda Husman et al., 2024). Moreover, the presence of mixed pixel scenarios hinders their precision in surface melt detection (Johnson et al., 2020).

UMelt, trained on Sentinel-1, combining the ASCAR and SSMIS datasets, demonstrates heightened sensitivity in detecting subtle melting events, particularly along the grounding line and within the Masson Island (de Roda Husman et al., 2024). However, the pursuit of comprehensive product coverage and a temporal resolution (every 12 h) necessitates a compromise in spatial resolution (500 m). The relatively simple architecture of U-Net makes it changeling to obtain multi-scale semantic information, which restricts the further improvement of accuracy (Zhang et al., 2021).

The proposed Attention DeepLabv3+ model has the ability to detect surface melt on multi-scale feature maps due to the ASPP and the attention mechanism can enhance the weights of the regions of surface melt. It accurately discerns the melting patterns of the Shackleton Ice Shelf (Fig. 7(a)), achieving an impressive accuracy of 95.97%, surpassing the baseline by 4.23% and the UMelt by 4.67%. While we acknowledge the presence of some misclassifications (highlighted in red boxes in Fig. 6(c)), and the Sentinel-1 data struggles to detect the surface melt with the presence of liquid water in ice regions (southeast of the Shackleton Ice Shelf, shown in Fig. 7) (Zheng et al., 2020; Liang et al., 2021a), which can both be attributed to the same low backscatter coefficients.

However, Our model demonstrates particular proficiency in capturing nuanced small-scale melt patterns, exemplified by the northern Shackleton Ice Shelf (Fig. 7(a)). In this context, UMelt tends to overestimate the surface meltwater, which is primarily attributed to the impact of training on lower-resolution ASCAT and SSMIS data. Our model performs well on detecting high-altitude mountainous regions surface melt (Figs. 6(c) and 6(d)). Additionally, the higher spatial resolution of our product (40 m) enhances its capability for precise detection of meltwater patterns and spatial distribution. This is crucial for advancing our understanding of ice shelf melting patterns and intricately delineating the significant impact of surface meltwater on global sea-level rise (Zhu et al., 2023a).

5.2. Performance evaluation for surface melt detection between deep learning and co-orbit normalization

Surface melt detection using SAR imagery faces challenges such as misidentifying ice crevasses, exposed ice, and misclassification due to radar shadow and radar imagery geometry (Liang et al., 2021a; de Roda Husman et al., 2024). The co-orbit normalization method applies reference imagery to normalize the images from the product period to mitigate these factors. However, reference-based methods present significant challenges when the absence of reference imagery and the pronounced movement occurring at ice sheets and shelves, where the former may lead to a decrease in the coverage range of data products, potentially stemming from the lack of winter reference images, while the latter may misinterpretation of displacement caused by ice shelves movement as surface melt.

Fig. 8 delineates our deep learning model and the traditional method results, demonstrating in areas affected by partial ice crevasses (highlighted by black boxes in Fig. 8(b) and (d)) and SAR geometry effects induced by variations in radar incidence angles due to terrain undulations (Fig. 8(c)). The primary aim of Liang et al. (2021a) is to rapidly obtain melt information across the Antarctic by co-orbit normalization. Therefore, precise spatial registration between the reference and product images has not been executed (Liang et al., 2021a), as it would notably degrade algorithm performance. This works well at most

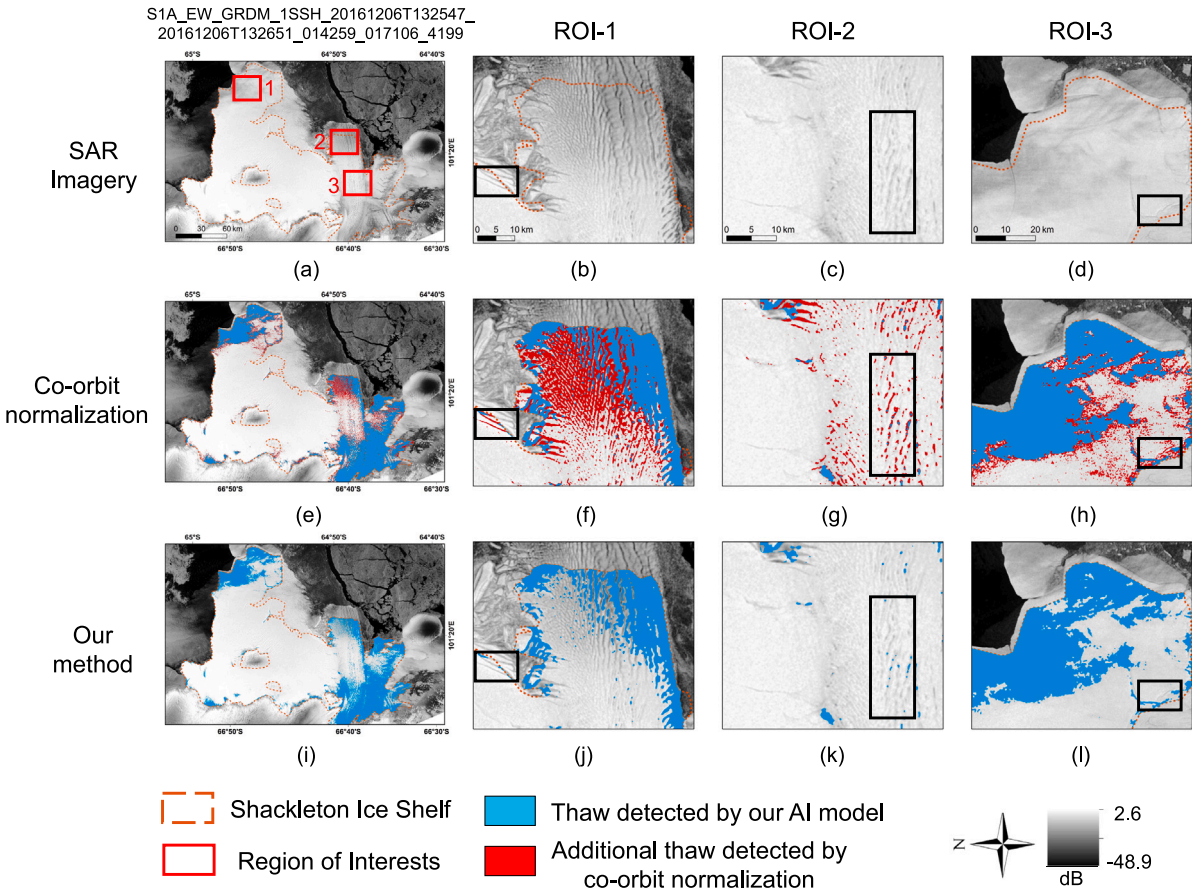

Fig. 8. Qualitative comparison of surface melt on the Shackleton Ice Shelf using our deep learning method and co-orbit normalization method from Liang et al. (2021a) on December 6, 2016.

Antarctic regions where the motions are generally not pronounced. However, as shown in Fig. 8, the method yielded erroneous classifications, especially at the leading edge of the Shackleton Ice Shelf with fast ice velocity and regions with pronounced terrain undulations (highlighted by black boxes in Fig. 8(f) and (g), respectively).

Contrarily, our approach effectively addressed these challenges (highlighted by black boxes in Fig. 8(j) and (k)) by employing the damage detection algorithm proposed by Izeboud and Lhermitte (2023). Additionally, the robust multi-scale semantic information extraction capability of DeepLabv3+ and the most vital features for melt detection derived from the CBAM mechanism facilitated more precise results. While we acknowledge that DL-based surface melt detection cannot completely eliminate the impact of ice crevasses and terrain undulations may still yield misclassifications, but it has achieved significant improvements compared with existing methods (Liang et al., 2021a; de Roda Husman et al., 2024).

5.3. Time series surface melt mapping for Larsen C ice shelf (LCIS)

The LCIS stands as the largest ice shelf along the eastern coast of the Antarctic Peninsula. It undergoes more notable rises in both oceanic and atmospheric temperatures when compared to other areas within the Antarctic region (Hubbard et al., 2016). In July 2017, LCIS witnessed the detachment of A-68, a colossal iceberg weighing 1 trillion tons and surpassing twice the size of Luxembourg, with an expansive area of 5800 km^2. Given this context, continuous and precise monitoring of surface melt on the LCIS assumes paramount importance as it represents a significant factor contributing to the ice shelf's collapse.

The surface melt map of LCIS for the period of 2019/2020 was generated using the proposed deep learning method (Fig. 9). The melting process of LCIS initiates near the continental section of the AP, exhibiting significantly earlier surface melt compared to the remainder of the ice shelf (Figs. 9(a) and 9(b)). This pattern starkly contrasts with its neighboring ice shelves, such as Wilkins and George VI ice shelves, where surface melt typically commences near the coastline influenced by warmer oceanic conditions (Zhu et al., 2023a). Gradually, the surface melt on LCIS progresses from north to south, nearing complete melt by December 19th and persisting until mid-March 2020. The southern section of the ice shelf experiences initial freezing, with only minimal surface melt remaining near the mainland by April 12th. The time-series surface melt mapping of Larsen C reveals a period of intense melting during 2019/2020, spanning over 100 days. These findings are consistent with Bevan et al. (2020), which reported the highest recorded melting in 40 years for the same period. This significant melt underscores the cessation of the apparent decline in ice shelf surface melt observed since the turn of the century.

5.4. Advantages, limitations and future work

5.4.1. Advantages

Compared to traditional surface melt detection methods, our work demonstrates major improvements in two key aspects: (1) Establishment of a substantial surface melt detection dataset encompassing the Antarctic region. (2) Introduction of a reference-free automated melt detection workflow utilizing deep learning. Through our proposed method, surface melt information can be directly obtained after basic

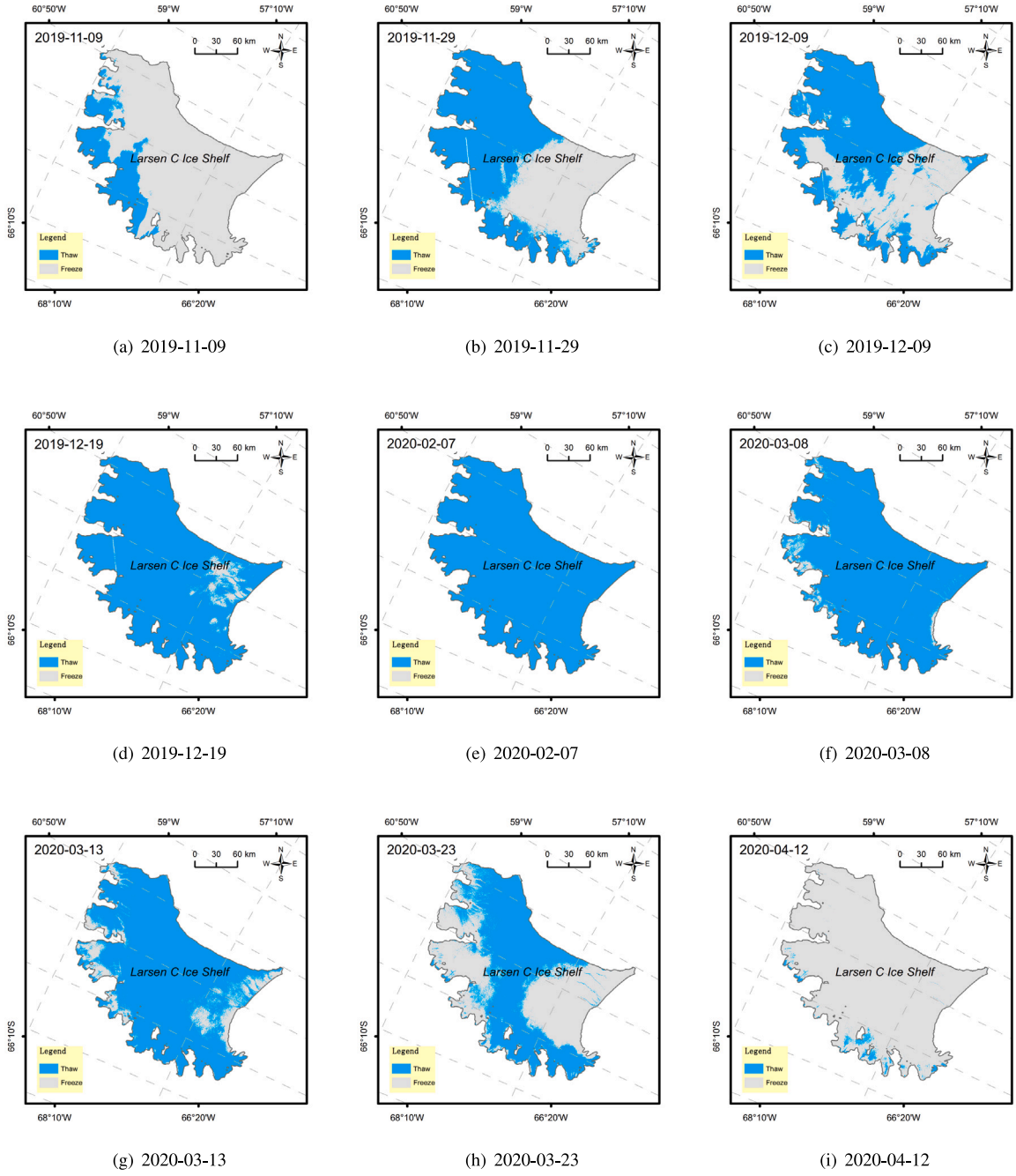

(a) 2019-11-09 (b) 2019-11-29 (c) 2019-12-09

(d) 2019-12-19 (e) 2020-02-07 (f) 2020-03-08

(g) 2020-03-13 (h) 2020-03-23 (i) 2020-04-12

Fig. 9. Time series surface melt information for Larsen C Ice Shelf in 2019/2020.

pre-processing of SAR images, eliminating the need for manual threshold selection that often introduces errors. The frequent occurrence of surface melt in complex terrains poses a considerable challenge for accurate detection (Wang et al., 2022). Moreover, the abundance of SAR imagery data presents a significant hurdle to efficient surface melt detection (Liang et al., 2021a). In response to these challenges, we introduce the Attention DeepLabv3+ to detect the surface melt, which can extract multi-scale semantic information to capture the distribution patterns of the image features from the ASPP layer, while the CBAM mechanisms enhances the expression ability of surface meltwater regions in the feature map, thus achieving precise classification of surface meltwater through continuous reinforcement learning and training. The results in our experiences demonstrate that the proposed Attention-DeepLabv3+ model effectively mitigates misjudgments caused by the aforementioned factors, including ice crevasses, radar shadows, and terrain undulations regions and reduces reliance on reference images, thereby improving the classification accuracy of surface meltwater

5.4.2. Limitations

While the proposed model offers notable advantages, the approach still has certain limitations. One is the requirement for substantial computing resources and a lengthy training time, with the ResNet-based Attention DeepLabv3+ model taking approximately 30 h to train. Moreover, the model encounters difficulties accurately identifying and classifying high-altitude regions with overlaps and shadows and surface

meltwater occurring on ice regions without snow cover, resulting in misjudgments under these specific conditions. Improving the model's capacity to handle such scenarios is an area that demands future research and development efforts. Finally, as our model is purely trained on Sentinel-1 imagery, its temporal resolution is constrained, which may miss the extraction and monitoring of some melting patterns of the ice shelves.

5.4.3. Prospects for improvement

There are several aspects in our existing model that offer opportunities for improvement. Firstly, augmenting the size of training samples stands as a straightforward approach to enhancing the network's accuracy by maximizing the model's potential. Secondly, Niu et al. (2023) has affirmed the potential use of utilizing Sentinel-2 optical imagery in detecting surface meltwater on the Amery Ice Shelf. This inspired us to integrate the SAR imagery and the optical imagery, incorporating with richer spectral information and higher spatial resolution to further enhance the bolster network's performance. Moreover, introducing a more sophisticated decoding layer in comparison to DeepLabv3+ or adopting novel network structures like the Transformer architecture (Dosovitskiy et al., 2020; Zhu et al., 2023b) presents an alternative pathway to augment the model's generalization capabilities.

6. Conclusion

The automated extraction of surface melt holds significant importance in monitoring ice sheet mass balance and investigating the mechanisms underlying ice shelf disintegration, particularly within the context of global climate change. In this study, we have introduced a novel surface melt detection dataset focused on the Antarctic, encompassing 9305 training samples along with corresponding labels derived from multi-temporal Sentinel-1 imagery. Our work involved the development of a reference-free automated framework for surface melt detection by integrating the attention mechanism into the DeepLabv3+ model. This approach streamlines the overall detection process while ensuring accuracy by reducing reliance on reference images. The successful application of our melt detection framework across diverse Antarctic surface conditions underscores its high level of generalization. This success augurs well for its potential wider applicability and relevance, extending beyond Antarctica to regions such as Greenland and Alaska.

CRediT authorship contribution statement

Qi Zhu: Writing – review & editing, Writing – original draft, Visualization, Methodology, Conceptualization. **Huadong Guo:** Supervision, Project administration. **Lu Zhang:** Writing – review & editing, Supervision, Funding acquisition, Conceptualization. **Dong Liang:** Writing – review & editing, Resources, Funding acquisition, Conceptualization. **Zherong Wu:** Writing – review & editing, Visualization, Methodology. **Sophie de Roda Husman:** Visualization, Validation, Resources. **Xiaobing Du:** Validation, Software.

Declaration of competing interest

The authors declare that they have no known competing financial interests or personal relationships that could have appeared to influence the work reported in this paper.

Data availability

Data will be made available on request.

Acknowledgments

This work was supported by the National Natural Science Foundation of China [grant number 42376246], the Key Research and Development Project of Guangxi [grant number GuikeAB24010046], and the Joint Funds of the National Natural Science Foundation of China [grant number U2268217]. The authors highly appreciate Editor-in-Chief Dr Jonathan Li, and two anonymous reviewers for the constructive comments. The authors also highly acknowledge Zhe Wu for the inspiring tutorial.

References

Antropova, Y.K., Komarov, A.S., Richardson, M., Millard, K., Smith, K., 2022. Detection of wet snow in the Arctic tundra from time-series fully-polarimetric RADARSAT-2 images. Remote Sens. Environ. 283, 113305.

Arthur, J.F., Stokes, C., Jamieson, S.S., Carr, J.R., Leeson, A.A., 2020. Recent understanding of Antarctic supraglacial lakes using satellite remote sensing. Prog. Phys. Geogr. Earth Environ. 44 (6), 837–869.

Banwell, A.F., Datta, R.T., Dell, R.L., Moussavi, M., Brucker, L., Picard, G., Shuman, C.A., Stevens, L.A., 2021. The 32-year record-high surface melt in 2019/2020 on the northern George VI Ice Shelf, Antarctic Peninsula. Cryosphere 15 (2), 909–925.

Benn, D.I., Cowton, T., Todd, J., Luckman, A., 2017. Glacier calving in Greenland. Curr. Clim. Change Rep. 3, 282–290.

Bergeron, J., Royer, A., Turcotte, R., Roy, A., 2014. Snow cover estimation using blended MODIS and AMSR-E data for improved watershed-scale spring streamflow simulation in Quebec, Canada. Hydrol. Process. 28 (16), 4626–4639.

Bevan, S., Luckman, A., Hendon, H., Wang, G., 2020. The 2020 Larsen C Ice shelf surface melt is a 40-year record high. Cryosphere 14 (10), 3551–3564.

Chen, L.-C., Zhu, Y., Papandreou, G., Schroff, F., Adam, H., 2018. Encoder-decoder with atrous separable convolution for semantic image segmentation. In: Proceedings of the European Conference on Computer Vision. ECCV, pp. 801–818.

de Roda Husman, S., Lhermitte, S., Bolibar, J., Izeboud, M., Hu, Z., Shukla, S., van der Meer, M., Long, D., Wouters, B., 2024. A high-resolution record of surface melt on Antarctic ice shelves using multi-source remote sensing data and deep learning. Remote Sens. Environ. 301, 113950.

Dosovitskiy, A., Beyer, L., Kolesnikov, A., Weissenborn, D., Zhai, X., Unterthiner, T., Dehghani, M., Minderer, M., Heigold, G., Gelly, S., et al., 2020. An image is worth 16x16 words: Transformers for image recognition at scale. arXiv preprint arXiv:2010.11929.

Du, S., Du, S., Liu, B., Zhang, X., 2021. Incorporating DeepLabv3+ and object-based image analysis for semantic segmentation of very high resolution remote sensing images. Int. J. Digit. Earth 14 (3), 357–378.

Gerrish, L., Fretwell, P., Cooper, P., 2020. High Resolution Vector Polylines of The Antarctic Coastline–version 7.3. Polar Data Centre, Natural Environment Research Council, uk Research e Innovation.

Gorelick, N., Hancher, M., Dixon, M., Ilyushchenko, S., Thau, D., Moore, R., 2017. Google earth engine: Planetary-scale geospatial analysis for everyone. Remote Sens. Environ. 202, 18–27.

Guo, H., Nativi, S., Liang, D., Craglia, M., Wang, L., Schade, S., Corban, C., He, G., Pesaresi, M., Li, J., et al., 2020. Big earth data science: an information framework for a sustainable planet. Int. J. Digit. Earth 13 (7), 743–767.

He, H., Xu, H., Zhang, Y., Gao, K., Li, H., Ma, L., Li, J., 2022. Mask R-CNN based automated identification and extraction of oil well sites. Int. J. Appl. Earth Obs. Geoinf. 112, 102875.

He, K., Zhang, X., Ren, S., Sun, J., 2016. Deep residual learning for image recognition. In: Proceedings of the IEEE Conference on Computer Vision and Pattern Recognition. pp. 770–778.

Howard, A., Sandler, M., Chu, G., Chen, L.-C., Chen, B., Tan, M., Wang, W., Zhu, Y., Pang, R., Vasudevan, V., et al., 2019. Searching for mobilenetv3. In: Proceedings of the IEEE/CVF International Conference on Computer Vision. pp. 1314–1324.

Hu, J., Shen, L., Sun, G., 2018. Squeeze-and-excitation networks. In: Proceedings of the IEEE Conference on Computer Vision and Pattern Recognition. pp. 7132–7141.

Hu, J., Zhang, T., Zhou, X., Jiang, L., Yi, G., Wen, B., Chen, Y., 2022. Extracting time-series of wet-snow facies in greenland using sentinel-1 SAR data on google earth engine. IEEE J. Sel. Top. Appl. Earth Obs. Remote Sens. 15, 6190–6196.

Hubbard, B., Luckman, A., Ashmore, D.W., Bevan, S., Kulessa, B., Kuipers Munneke, P., Philippe, M., Jansen, D., Booth, A., Sevestre, H., et al., 2016. Massive subsurface ice formed by refreezing of ice-shelf melt ponds. Nat. Commun. 7 (1), 1–6.

Izeboud, M., Lhermitte, S., 2023. Damage detection on Antarctic ice shelves using the normalised radon transform. Remote Sens. Environ. 284, 113359.

Jakobs, C., Reijmer, C., Van den Broeke, M., Van de Berg, W., Van Wessem, J., 2021. Spatial variability of the snowmelt-albedo feedback in Antarctica. J. Geophys. Res. Earth Surf. 126 (2), e2020JF005696.

Johnson, A., Fahnestock, M., Hock, R., 2020. Evaluation of passive microwave melt detection methods on Antarctic Peninsula ice shelves using time series of Sentinel-1 SAR. Remote Sens. Environ. 250, 112044.

Liang, D., Guo, H., Zhang, L., Cheng, Y., Zhu, Q., Liu, X., 2021a. Time-series snowmelt detection over the Antarctic using Sentinel-1 SAR images on google earth engine. Remote Sens. Environ. 256, 112318.

Liang, D., Guo, H., Zhang, L., Wang, M., Wang, L., Liang, L., Shirazi, Z., 2021b. Analyzing Antarctic ice sheet snowmelt with dynamic big earth data. Int. J. Digit. Earth 14 (1), 88–105.

Liang, L., Li, X., Zheng, F., 2019. Spatio-temporal analysis of ice sheet snowmelt in Antarctica and Greenland using microwave radiometer data. Remote Sens. 11 (16), 1838.

Ma, P., Wu, Z., Zhang, Z., Au, F.T., 2024a. SAR-transformer-based decomposition and geophysical interpretation of InSAR time-series deformations for the Hong Kong-Zhuhai-Macao bridge. Remote Sens. Environ. 302, 113962.

Ma, P., Yu, C., Jiao, Z., Zheng, Y., Wu, Z., Mao, W., Lin, H., 2024b. Improving time-series InSAR deformation estimation for city clusters by deep learning-based atmospheric delay correction. Remote Sens. Environ. 304, 114004.

Nair, V., Hinton, G.E., 2010. Rectified linear units improve restricted boltzmann machines. In: ICML.

Niu, L., Tang, X., Yang, S., Zhang, Y., Zheng, L., Wang, L., 2023. Detection of Antarctic surface meltwater using Sentinel-2 remote sensing images via U-net with attention blocks: A case study over the Amery Ice Shelf. IEEE Trans. Geosci. Remote Sens..

Trusel, L., Frey, K.E., Das, S.B., 2012. Antarctic surface melting dynamics: Enhanced perspectives from radar scatterometer data. J. Geophys. Res.: Earth Surf. 117 (F2).

Vaswani, A., Shazeer, N., Parmar, N., Uszkoreit, J., Jones, L., Gomez, A.N., Kaiser, Ł., Polosukhin, I., 2017. Attention is all you need. Adv. Neural Inf. Process. Syst. 30.

Wang, Y., Gao, L., Hong, D., Sha, J., Liu, L., Zhang, B., Rong, X., Zhang, Y., 2021. Mask DeepLab: End-to-end image segmentation for change detection in high-resolution remote sensing images. Int. J. Appl. Earth Obs. Geoinf. 104, 102582.

Wang, X.-D., Li, X.-W., Wang, C., Li, X.-G., 2018. Antarctic ice-sheet near-surface snowmelt detection based on the synergy of SSM/I data and QuikSCAT data. Geosci. Front. 9 (3), 955–963.

Wang, X., Qiu, Y., Zhang, Y., Lemmetyinen, J., Cheng, B., Liang, W., Leppäranta, M., 2022. A lake ice phenology dataset for the Northern Hemisphere based on passive microwave remote sensing. Big Earth Data 6 (4), 401–419.

Woo, S., Park, J., Lee, J.-Y., Kweon, I.S., 2018. Cbam: Convolutional block attention module. In: Proceedings of the European Conference on Computer Vision. ECCV, pp. 3–19.

Wu, Z., Ma, P., Zheng, Y., Gu, F., Liu, L., Lin, H., 2023. Automatic detection and classification of land subsidence in deltaic metropolitan areas using distributed scatterer InSAR and oriented R-CNN. Remote Sens. Environ. 290, 113545.

Zhang, E., Liu, L., Huang, L., Ng, K.S., 2021. An automated, generalized, deep-learning-based method for delineating the calving fronts of Greenland glaciers from multi-sensor remote sensing imagery. Remote Sens. Environ. 254, 112265.

Zheng, L., Zhou, C., Wang, K., 2020. Enhanced winter snowmelt in the Antarctic Peninsula: Automatic snowmelt identification from radar scatterometer. Remote Sens. Environ. 246, 111835.

Zhu, Q., Guo, H., Zhang, L., Liang, D., Liu, X., Zhou, H., Gou, Y., 2023a. High-resolution spatio-temporal analysis of snowmelt over Antarctic Peninsula ice shelves from 2015 to 2021 using SAR images. Int. J. Digit. Earth 16 (1), 825–846.

Zhu, Q., Guo, H., Zhang, L., Liang, D., Wu, Z., Liu, Y., Lv, Z., 2023b. GLA-STDeepLab: SAR enhancing glacier and ice shelf front detection using swin-TransDeepLab with global-local attention. IEEE Trans. Geosci. Remote Sens..

Zhu, X.X., Montazeri, S., Ali, M., Hua, Y., Wang, Y., Mou, L., Shi, Y., Xu, F., Bamler, R., 2021. Deep learning meets SAR: Concepts, models, pitfalls, and perspectives. IEEE Geosci. Remote Sens. Mag. 9 (4), 143–172.